

## Hybrid GA- SVM for feature selection to improve Automatic Bayesian classification of Brain MRI Slice

R. Karuppathal<sup>1</sup>, Dr.V. Palanisamy<sup>2</sup>

<sup>1</sup>. Associate Professor, PSNA College of Engineering and Technology, Dindigul-624 622, India

<sup>2</sup>. Principal, Info Institute of Engineering, Coimbatore-641 107, India.

[karuppathal.r@gmail.com](mailto:karuppathal.r@gmail.com)<sup>1</sup>, [vpsamyin@gmail.com](mailto:vpsamyin@gmail.com)<sup>2</sup>

**Abstract:** The major tissues with in a Brain are identified by Magnetic resonance imaging (MRI) based on nuclear magnetic response MRI is a non invasive method for imaging. A intelligent optimization technique to identify normal and abnormal slices of brain MRI data. The manual interpretation of tumor slices based on visual examination by Radiologist/physician may lead to missing diagnosis when a large number of MRIs are analyzed. To avoid the human error, an automatic Bayesian optimization system is proposed which caters the need for optimization of image slices after identifying abnormal MRI volume, for tumor identification. In this research work, advanced optimization techniques based on Hybrid Genetic Algorithm Support Vector Machines (Hybrid GA-SVM) are proposed and applied to brain image slices optimization using features selection from slices. From this analysis, it is observed that the proposed method using Hybrid GA-SVM optimizer outperformed all other existing methodologies.

[R. Karuppathal, V. Palanisamy. **Hybrid GA- SVM for feature selection to improve Automatic Bayesian classification of Brain MRI Slice.** *Life Sci J* 2013;10(2):2273-2280] (ISSN:1097-8135). <http://www.lifesciencesite.com>. 318

**Keywords:** Brain MRI Slices, brain tumor, hybrid GA-SVM.

### 1. Introduction

Brain is the kernel part of the body. Brain has a very complex structure. Brain is hidden from direct view by the protective skull. This skull gives brain protection from injuries. Brain can be affected by a problem which cause change in its normal structure and its normal behavior .This problem is known as brain tumor. Brain tumor causes the abnormal growth of the cells in the brain. The cells which supplies the brain in the arteries are tightly bound together thereby routine laboratory test are inadequate to analyze the chemistry of brain. Computed tomography and magnetic resonance imaging are two imaging modalities that allow the doctors and researchers to study the brain by looking at the brain non-invasively.

The field of medical imaging gains its importance with increase in the need of automated and efficient diagnosis in a short period of time. Computer and Information Technology are very much useful in medical image processing, medical analysis and optimization. Medical images are usually obtained by X-rays and recent years by Magnetic Resonance (MR) imaging. Magnetic Resonance Imaging (MRI) is used as a valuable tool in the clinical and surgical environment because of its characteristics like superior soft tissue differentiation, high spatial resolution and contrast. It does not use harmful ionizing radiation to patients.

Magnetic Resonance Imaging (MRI) is a medical imaging technique. Radiologist used it for the visualization of the internal structure of the body.

MRI provides rich information about human soft tissues anatomy. MRI helps for diagnosis of the brain tumor. Images obtained by the MRI are used for analyzing and studying the behavior of the brain. Image intensity in MRI depends upon four parameters. One is proton density (PD) which is determined by the relative concentration of water molecules. Other three parameters are T1, T2, and T2\* relaxation, which reflect different features of the local environment of individual protons. Ones the brain images acquired they are optimized as normal and abnormal. For optimization of the images different features of the image are extracted. These features are used for optimizing the brain MR image as normal and abnormal. The sensitivity of the human eye in interpreting large numbers of images decreases with increasing number of cases, particularly when only a small number of slices are affected. The MRI may contain both normal slices and defective slices. The defective or abnormal slices are identified and separated from the normal slices and then these defective slices are further investigated for the detection of tumor tissues.

Brain MRI in which an SVM optimizer was used for normal and abnormal slices optimization with statistical features. The latest development in data optimization research has focused more Hybrid GA (SVM) Support Vector Machines because several recent studies have reported that Hybrid GA-SVM generally is able to deliver higher optimization accuracy than the other existing data optimization algorithms. The

categorization of slices into normal and abnormal is done using statistical features of images such as mean, variance, and co occurrence based textural features of images such as energy, entropy, difference moment, inverse difference moment and correlation. For comparative analysis, SVM Optimizer with linear and nonlinear type of kernels, the RBF, MLP and K-NN optimizers are also implemented using the same data sets. The motivation behind this paper is to develop a machine optimization process for evaluating the optimization performance of different optimizers to this problem in terms of statistical performance measure.

The motivation behind this paper is to develop a machine optimization process for evaluating the optimization performance of different optimizers to this problem in terms of statistical performance measure. Our proposed technique is fully automatic and robust. No prior knowledge of the image is required about its feature, contents, type and model. Proposed system is very accurate system for diagnosing the brain tumor.

**2. Material and Methods**

**2.1 Image MRI**

Magnetic Resonance Imaging (MRI) uses magnetic energy and radio waves to create images (“slices”) of the human body. MR imaging measures the magnetic properties of nuclei within the body tissues. The energy absorbed by the nuclei is then released, returning the nuclei to their initial state of equilibrium and this transmission of energy by the nuclei is observed as the MRI signal. MR images are generated by the resonating nuclei for each spatial location. The image gray level in MRI mainly depends on three tissue parameters viz., proton density (PD), spin-lattice (T1) and spin-spin (T2) relaxation time [22]. Generally, for most of the soft tissues in the body, the proton density is very homogenous but may exhibit higher intensity for gray matter. T1 and T2 are sensitive to the local environment; they are used to characterize different tissue types. T1, T2 and PD type images are mostly used by different researchers [23, 24] for different MR applications.

**2.2 Feature GLCM**

A number of texture features may be extracted from the GLCM We use the following notation: G is the number of gray levels used.  $\mu$  is the mean value of P.  $\mu_x$ ,  $\mu_y$ ,  $\sigma_x$  and  $\sigma_y$  are the means and standard deviations of  $P_x$  and  $P_y$ .  $P_x(i)$  is the  $i$ th entry in the marginal-probability matrix obtained by summing the rows of  $P(i, j)$

$$P_x(i) = \sum_{j=0}^{G-1} P(i, j) \quad P_y(j) = \sum_{i=0}^{G-1} P(i, j)$$

$$\begin{aligned} \mu_x &= \sum_{i=0}^{G-1} i \sum_{j=0}^{G-1} P(i, j) = \sum_{i=0}^{G-1} i P_x(i) \\ \mu_y &= \sum_{j=0}^{G-1} j \sum_{i=0}^{G-1} P(i, j) = \sum_{j=0}^{G-1} j P_y(j) \\ \sigma_x^2 &= \sum_{i=0}^{G-1} (i - \mu_x)^2 \sum_{j=0}^{G-1} P(i, j) = \sum_{i=0}^{G-1} (P_x(i) - \mu_x(i))^2 \\ \sigma_y^2 &= \sum_{j=0}^{G-1} (j - \mu_y)^2 \sum_{i=0}^{G-1} P(i, j) = \sum_{j=0}^{G-1} (P_y(j) - \mu_y(j))^2 \end{aligned}$$

and

$$P_{x+y}(k) = \sum_{i=0}^{G-1} \sum_{j=0}^{G-1} P(i, j)$$

$i+j=k$   
for  $k=0, 1, \dots, 2(G-1)$

$$P_{x-y}(k) = \sum_{i=0}^{G-1} \sum_{j=0}^{G-1} P(i, j)$$

$i-j=k$   
for  $k=0, 1, \dots, G-1$

The following features are used  
Homogeneity, Angular Second Moment (ASM)

$$ASM = \sum_{i=0}^{G-1} \sum_{j=0}^{G-1} \{P(i, j)\}^2$$

ASM is a measure of homogeneity of an image. A homogeneous scene will contain only a few gray levels, giving a GLCM with only a few but relatively high values of  $P(i, j)$ . Thus, the sum of squares will be high.

Contrast

$$CONTRAST = \sum_{n=0}^{G-1} n^2 \left\{ \sum_{i=1}^n \sum_{j=1}^n P(i, j) \right\}, |i-j|=n$$

This measure of contrast or local intensity variation will favour contributions from  $P(i, j)$  away from the diagonal, i.e.  $i \neq j$ .

Local Homogeneity, Inverse Difference Moment (IDM)

$$IDM = \sum_{i=0}^{G-1} \sum_{j=0}^{G-1} \frac{1}{1+(i-j)^2} P(i, j)$$

IDM is also influenced by the homogeneity of the image. Because of the weighting factor  $(1+(i-j)^2)^{-1}$  IDM will get small contributions from inhomogeneous areas ( $i \neq j$ ). The result is a low IDM value for inhomogeneous images, and a relatively higher value for homogeneous images.

Entropy

$$ENTROPY = - \sum_{i=0}^{G-1} \sum_{j=0}^{G-1} P(i, j) \times \log(P(i, j))$$

Inhomogeneous scenes have low first order entropy, while a homogeneous scene has high entropy.

Correlation

$$CORRELATION = \frac{\sum_{i=0}^{G-1} \sum_{j=0}^{G-1} (i \times j) \times P(i, j) - (\mu_x \times \mu_y)}{\sigma_x \times \sigma_y}$$

Correlation is a measure of gray level linear dependence between the pixels at the specified positions relative to each other.

Sum of Squares, Variance

$$\text{VARIANCE} = \sum_{i=0}^{g-1} \sum_{j=0}^{g-1} (i - \mu)^2 P(i, j)$$

This feature puts relatively high weights on the elements that differ from the average value of P (i, j).

Sum Average

$$\text{AVER} = \sum_{i=0}^{g-1} i P_{x+y}(i)$$

Sum Entropy

$$\text{SENT} = - \sum_{i=0}^{g-1} P_{x+y}(i) \log(P_{x+y}(i))$$

Difference Entropy

$$\text{DENT} = - \sum_{i=0}^{g-1} P_{x+y}(i) \log(P_{x+y}(i))$$

Inertia

$$\text{INERTIA} = \sum_{i=0}^{g-1} \sum_{j=0}^{g-1} (i - j)^2 \times P(i, j)$$

Cluster Shade

$$\text{SHADE} = \sum_{i=0}^{g-1} \sum_{j=0}^{g-1} (i + j - \mu_x - \mu_y)^3 \times P(i, j)$$

Cluster Prominence

$$\text{PROM} = \sum_{i=0}^{g-1} \sum_{j=0}^{g-1} (i + j - \mu_x - \mu_y)^4 \times P(i, j)$$

### 2.3 Feature Selection

#### a. Genetic Algorithm

GA is represented by a chromosome and the GA keeps a set (population) of chromosomes. Each element of a chromosome is referred to as a gene. The population evolves through a number of generations. Each generation is performed as follows. First, two solutions are selected in the population based on a certain probability distribution; they are called parent chromosomes. Then, the crossover operation produces an offspring chromosome by combining the parents. The mutation operation then modifies the offspring chromosome with a low probability. The offspring can be locally improved by any other algorithm or heuristic. A generation is completed by replacing one of the members in the population with the offspring. A considerable number of generations are run until a user-defined convergence criterion is reached.

Finally, the GA returns the optimized parameters or variables in the population as the solution [11].

#### b. Support Vector Machine

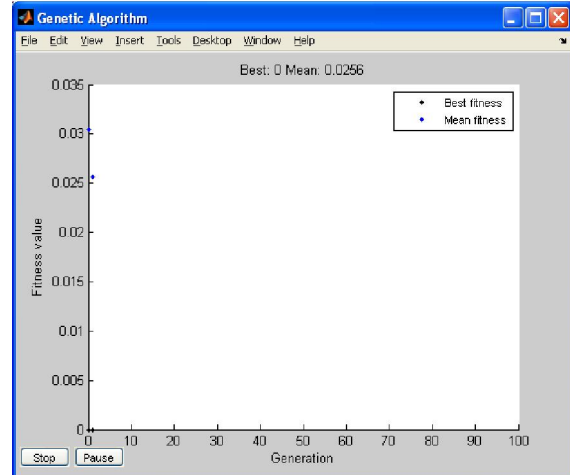


Figure 1. Fitness calculation

SVMs are a set of novel machine learning methods for optimization and regression. In SVM, training is performed in a way such to obtain a quadratic programming (QP) problem. The solution to this QP problem is global and unique. For Empirical data  $(x_1, y_1), \dots, (x_m, y_m) \in \mathbb{R}^n \times \{-1, +1\}$  that are mapped by  $\phi: \mathbb{R}^n \rightarrow F$  into a "feature space", the linear hyper planes that divide them into two labeled classes can be mathematically represented as:

$$w \times \phi(x) + b = 0 \quad w \in \mathbb{R}^n, b \in \mathbb{R} \quad (1)$$

To construct an optimal hyper plane with maximum-margin and bounded error in the training data (soft margin), the following QP problem is to be solved:

$$\min_{w, b} \frac{1}{2} |w|^2 + C \sum_{i=1}^m \xi_i$$

$$y_i (w \times \phi(x) + b) \geq 1 - \xi_i, \quad i = 1, 2, \dots, m \quad (2)$$

The first term in cost function (2) makes maximum margin of separation between classes, and the second term provides an upper bound for the error in the training data. The constant  $C \in [0, \infty)$  creates a tradeoff between the number of optimized samples in the training set and separation of the rest samples with maximum margin. A way to solve (2) is via its Lagrange function. Given a kernel  $K(x_i, y_j) = \phi(x_i) \cdot \phi(x_j)$  the Lagrange function of (2) is simplified to:

$$\max \sum_{i=1}^m \alpha_i - \frac{1}{2} \sum_{i=1}^m \sum_{j=1}^m \alpha_i \alpha_j y_i y_j K(x_i, x_j) \quad (3)$$

$$w = \sum_{i=1}^m y_i \alpha_i \phi(x_i), \sum_{i=1}^m \alpha_i y_i = 0, 0 \leq \alpha_i \leq C, \forall_i \quad (4)$$

From eq. (1) it is seen that the optimal hyper plane in the feature space can be written as the linear combination of training samples with  $\alpha_i \neq 0$ . These informative samples, known as *support vectors*, construct the decision function of the optimizer based on the kernel function:

$$f(x) = \text{sgn} \left\{ \sum_{i=1}^m y_i \alpha_i k(x, x_i) \right\} + b \quad (5)$$

Kernel functions in SVMs are selected based on the data structure and type of the boundaries between the classes. The representative and widely applied kernel function based on Euclidean distance is the radial basis function (RBF) kernel, also known as the Gaussian kernel [13]:

$$K^{\text{RBF}}(x_i, x_j) = \exp(-\gamma \|x_i - x_j\|^2) \quad (6)$$

Where  $\gamma > 0$  is the RBF kernel parameter. The RBF kernel induces an infinite-dimensional kernel space, in which all image vectors have the same norm, and the kernel width parameter  $\gamma$  controls the scaling of the mapping [13]. This paper employs LIBSVM [14], a library for support vector machines, as the core SVM optimizer and conducts multiclass optimization using the “One Against One” or OAO method.

*c. GA Optimization*

A hybrid approach of GA-SVM is used to globally optimize SVM hyper-parameters for the following Dual Lagrangian Optimization (DLO) problem:

$$L = \sum_{i=1}^m \alpha_i - \frac{1}{2} \sum_{i=1}^m \sum_{j=1}^m \alpha_i \alpha_j y_i y_j k(x_i, x_j) \quad (7)$$

Since the SVM uses the RBF kernel, the hyper-parameters include: Lagrange multipliers  $(\alpha_1, \alpha_2, \dots, \alpha_i)$ , C and  $\gamma$ . In GA for optimization, all corresponding parameters are directly coded to form a chromosome. Consequently, the chromosome  $X$  is represented as  $X = \{ \alpha_1, \alpha_2, \dots, \alpha_i, p1, p2 \}$ , where  $i$  represents the number of training features,  $p1$  and  $p2$  denote “C” the cost of errors and “ $\gamma$ ” is the RBF kernel parameter.

The hybrid GA-SVM process is based on the survival principle of the fittest member in a population, which retains its genetic information by passing it on from generation to generation. The process of GA for SVM hyper-parameter optimization is described as follows:

*Initialization:* Generate a random initial population of  $n$  chromosomes (suitable solutions for the problem).

*Fitness Evaluation:* Evaluate the fitness  $f(x)$  of each chromosome  $x$  in the problem. In this problem, the DLO function in eq. (7) is used as the fitness function.

*Selection:* Select two parent chromosomes according to their fitness for reproduction using the Roulette Wheel method. The area of the slice is proportional to the chromosome fitness ratio  $Rf$  and is calculated using:

$$R_f = \frac{f(i)}{\sum_{i=1}^N f(i)} \times 100\% \quad (8)$$

where  $f(i)$  is the fitness of the  $i$ th chromosome.

*Crossover:* Form new offspring (children) from the parents using a single-point crossover probability.

*Mutation:* Mutate the new offspring at each position using a uniform mutation probability measure.

*Next Generation:* Form the PPD for the next generation.

*Test:* If the number of generations exceeds the initialized value, then stop and return the best chromosomes in the current population as the solution.

*Loop:* Go to step 2.

For each of the 10 pairs of  $(C, \gamma)$  obtained from the PPD, performance was measured by training 70% of the optimizer data and testing the other 30%. For GA optimization, several parameters were tested. Experimentally it was found that GA parameters illustrated in Table II, were the most suitable parameters for obtaining the highest SVM cross-validation (CV) accuracy and fraud detection hit-rate.

GA parameters used for SVM Hyper Parameter Optimization

GA Parameter	Value
Maximum Generation	500
Population Size	1000
Crossover Rate	0.8
Mutation Rate	0.025

From all the 10 pairs of  $(C, \gamma)$ , optimal hyper-parameters selected were:  $C = 20.4726$  and  $\gamma = 0.2608$ . The hybrid GASVM optimization and training engine is illustrated. Using this  $(C, \gamma)$  parameter set, the highest 10-fold CV accuracy achieved was 92.58%. The reason for using 10-fold CV is to ensure the model does not over fit the training data.

**2.4 Bayesian Classification**

In MR data sets, partial volume effects occur in pixels along the borders between distinct tissues. This is because of the finite volume of tissue represented

by each pixel. Assuming that there is no intensity non uniformity across homogeneous tissue, pure tissue intensity can be reasonably modeled by a Gaussian distribution. This is a common assumption that forms the basis of nearly all image segmentation techniques. Regions containing a mixture of tissue have intensities that reflect the combination of all tissues within each pixel (partial volume averaging).

The method of segmentation presented herein addresses these partial volume effects, accepting that segmentation is not binary in nature from pixel to pixel; boundaries do not normally align with the sampling grid at the resolution of the imaging sequence. Common to all approaches to statistical analysis of MR data in the literature, we started by assuming that all pure tissues can be modeled by a single distribution with fixed mean. To help ensure this, each data set was corrected for intensity non uniformity due to radio-frequency field in homogeneity by using a post processing technique. Finally, for the purpose of this study, all materials in the sampled region of interest were identified as brain, CSF, or tumor tissue. In some situations, such as pixels containing blood or other non modeled tissues, this resulted in systematic errors in the measured values. However, systematic errors can be ignored if the primary goal is case-to-case growth rate monitoring (as systematic errors cancel in a computed difference). The main requirements for such a measurement process are high repeatability and sensitivity to change. We assessed both of these issues by using a combination of patient data and statistical phantoms.

The Bayesian approach to data analysis allows us to assess the most likely distribution of tissue proportions within a pixel. The tissue volume model is composed of terms for pure tissue and partial volumes. The pure tissues follow convention and use Gaussian distributions. The partial volume model is an extension of the work of Laidlaw et al (12). To make Bayesian estimation of most likely volume fraction possible, we had to model partial volumes from two tissues as two separate distributions of the expected volume fraction of each tissue within the volume. The linearity of the Bloch equations combined with our previous assumption regarding the expected Gaussian distribution of the pure tissue rendered partial volume curves for each tissue, which were triangular distributions convolved with the pure tissue distribution (Figure 1). This allowed us to write down an equation for the total amount of each tissue within a particular region of the image as a sum of pure and partial volume contributions weighted with the relative proportions of each (Equation 1)

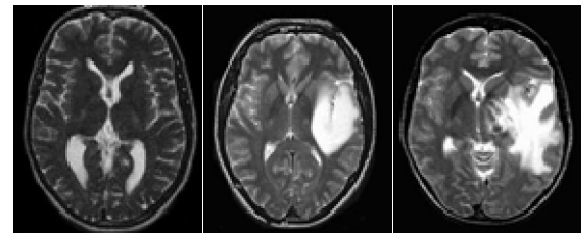
$$P_{tot}(g) = f_1P_1(g) + f_2P_2(g) + f_3P_3(g) + f_{1-2}P_{1-2}(g) + f_{2-1}P_{2-1}(g) + f_{2-3}P_{2-3}(g) + f_{3-2}P_{3-2}(g),$$

where  $f_i$  is the weight given to each of the basic functions in the fit.  $P_i$  is the probability that a given gray level,  $g$ , has come from the basis function corresponding to tissue subclass  $i$  (1 \_ pure CSF, 2 \_ pure brain tissue, 3 \_ pure tumor tissue, 1-2 \_ CSF in partial volume pixels with brain tissue, 2-1 \_ brain tissue I partial volume pixels with CSF, etc)

Having established the model, we must now determine the free parameters, which are the expected mean value of the pure tissues and the relative proportions of each distribution. A simplex algorithm was used to optimize the 2 fit between an image's intensity histogram and the regional model,  $P_{tot}(g)$  (23).

### 3. Results and Discussion

In order to verify the effectiveness and robustness of GA-SVM optimizer, experiments were performed on MR images. Our proposed hybrid techniques are implemented on a real human brain dataset. The input dataset consist images: 18 images are normal, 17 malignant tumors suffering from a low grade Glioma, Meningioma and 91 benign tumors suffering from a Bronchogenic Carcinoma, Glioblastoma multiform, Sarcoma and Grade IV tumors. These normal and pathological benchmark images used for optimization are axial, T2-weighted of 256\*256 sizes and acquired at several positions of the transaxial planes. These images were collected from the Harvard Medical School website [26]. We have considered that all images belonging to seven persons (four men and three women). Their ages vary between 22 and 81 years. The determination of MR tumor type, which can be achieved by the histopathological analysis of biopsies, was considered as the gold standard for the optimization of images. A typical representative MR image of normal, benign and malignant tumor is shown in Figure.



a) Normal Brain b) Benign tumor c) Malignant tumor

In this section, we present the performance evaluation methods used to evaluate the proposed approaches. We assess the performance of the proposed method in terms of sensitivity, specificity

and accuracy. The three terms are defined in Equations,

$$\begin{aligned} \text{Sensitivity} &= \text{TP}/(\text{TP}+\text{FN}) \text{ 100\%} \\ \text{Specificity} &= \text{TN}/(\text{TN}+\text{FN}) \text{ 100\%} \\ \text{Accuracy} &= (\text{TP}+\text{TN})/(\text{TP}+\text{TN}+\text{FP}+\text{FN}) \text{ 100\%} \end{aligned}$$

Where:

TP(True Positives)= correctly optimized positive cases,  
 TN (True Negative) = correctly optimized negative cases,  
 FP (False Positives) = incorrectly optimized negative cases.  
 FN (False Negative) = incorrectly optimized positive cases.

Table1. Confusion matrix for Bayesian Classification

	Normal	Benign	Malignant
Normal	18	5	0
Benign	2	17	6
Malignant	1	10	91

To evaluate the tumor’s detection accuracy, the algorithm performance is compared with the decisions made by four expert radiologist experts. For brain tumor optimization, we first optimize the brain into normal or abnormal. Then also optimize abnormal image to benign or malignant. The experiment results for normal and abnormal image to benign or malignant optimizations are listed in Table 1. According to these results, a optimization rate is obtained in Table 2.

Table 2. Optimizer Performance for Bayesian Classification

	Value
Correct rate	0.8400
Error Rate	0.1600
LastCorrectRate	0.8400
Last Error Rate	0.1600
Inconclusive Rate	0
Classified Rate	1
Sensitivity	0.7826
Specificity	0.9764
Positive PredictiveValue	0.8571
Negative Predictive Value	0.9612
Positive Likelihood	33.1304
Negative Likelihood	0.2227
Prevalence	0.1533

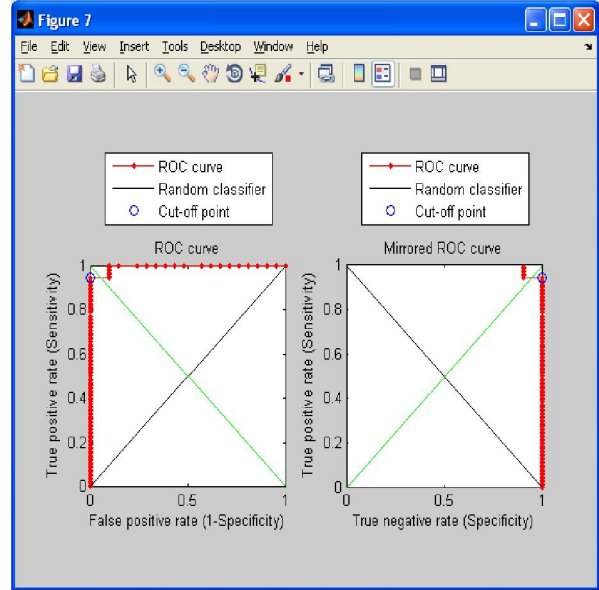


Figure. Curve evaluation

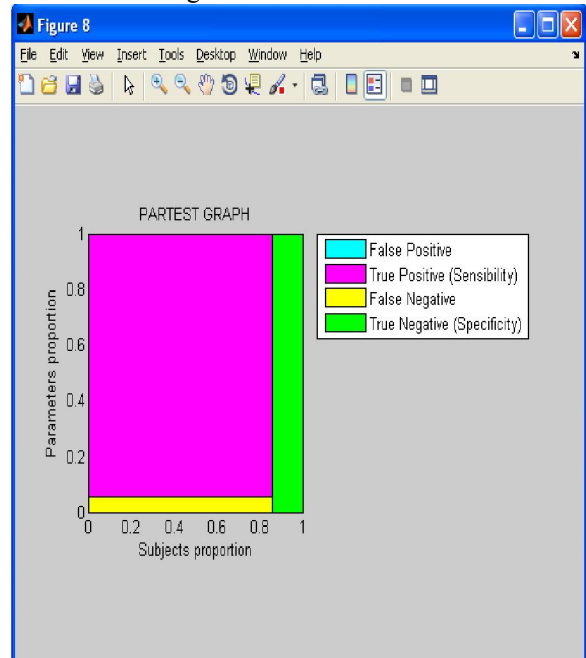


Figure. Partest graph

The performance evaluations are shown in above figures. This comparison shows that our system has high optimization accuracy and less computation due to the feature extraction. Hence the experimental results show that the accuracy results of optimization of proposed approach are better than the other one lacking the decomposition stage for optimization of the human brain tumor. This makes our approach an efficient clinical image analysis tool for doctors or radiologists to optimize MRI tumor and to further obtain MRI tumor location and Vol. estimation.

#### 4. Conclusion

In this paper, the computer based technique for Automatic Bayesian optimization of MRI slices as normal or abnormal with various MR image features using different optimizers is proposed. This research involves using Hybrid GA-SVM to optimize the input which is MRI Brain into normal and abnormal optimization. The performances of the optimizers in terms of statistical measures such as sensitivity, specificity and optimization accuracy are analyzed.

The results indicated that the Hybrid GA-SVM approach yielded the better performance when compared to other optimizers. It suggests that Hybrid GA-SVM is a promising technique for image optimization in a medical imaging application. It can be used in computer aided intelligent health care systems. This automated analysis system could be further used for optimization of images with different pathological condition, types and disease status.

#### References

1. Yamamoto M, Hagiwara S, Ide M, Jimbo M, Arai Y, Ono Y. Conservative management of acoustic neurinomas: prospective study of long-term changes in tumor volume and auditory function. *Minim Invasive Neurosurg* 1998; 41:86–92.
2. Provenzale JM, Mukundan S, Baroriak DP. Diffusion-weighted and perfusion MR imaging for brain tumor characterization and assessment of treatment response. *Radiology* 2006; 239:632–649.
3. Wang Q, Liacouras EK, Miranda E, Kanamala US, Megalooikonomou V. Classification of brain tumors using MRI and MRS. In: Proceedings of the SPIE Conference on Medical Imaging, 2007.
4. Mayerhoefer ME, Szomolanyi P, Jirak D, Materka A, Trattnig S. Effects of MRI acquisition parameter variations and protocol heterogeneity of the results of texture analysis and pattern discrimination: an application-oriented study. *Med Phys* 2009; 36:1236–1243.
5. M. C. Clark, L. O. Hall, D. B. Goldgof, L. P. Clarke, R. P. Velthuizen, and M. S. Silbiger, "MRI Segmentation using Fuzzy Clustering Techniques", IEEE Engineering in Medicine and Biology, pp. 730-742, 1994.
6. D. Selvathi, R.S. Ram Prakash, Dr. S. Thamarai Selvi, "Performance Evaluation of Kernel Based Techniques for Brain MRI Data Classification" International Conference on Computational Intelligence and Multimedia Applications 2007.
7. Jenkinson M, Smith SA. Global optimisation method for robust affine registration of brain images. *Med Image Anal* 2001; 5:143–156.
8. Smith SM: BET: brain extraction tool. FMRIB technical report TR00SMS26.
9. Lacey T. *Neuro-Imaging Analysis Centre*. Manchester, England: University of Manchester; 2000.
10. Slattery W, Brackmann D, Hitselberger W. Hearing preservation in neurofibromatosis type 2. *Am J Otol* 1998; 19:638–643?
11. Shirato H, Sakamoto T, Sawamura Y, et al. Comparison between observation policy and fractionated stereotactic radiotherapy (SRT) as an initial management for vestibular schwannoma.
12. Kovacsovics B, Davidsson L, Harder H, Magnuson B, L MRI screening of the cerebellopontine angle and inner ear with fast spin-echo T2 technique. *Arch Ital Biol* 2000.
13. Vokurka EA, Thacker NA, Jackson A. A fast model independent method for automatic correction of intensity nonuniformity in MRI data. *J Magn Reson Imaging* 1999; 10:550–562.
14. Laidlaw D, Fleischer K, Barr A. Partial-volume Bayesian classification of material mixtures in MR volume data using voxel histograms. *IEEE Trans Med Imag* 1998; 17:74–86.
15. Fucci MJ, Buchman CA, Brackmann DE, Berliner KI. Acoustic tumor growth: implications for treatment choices. *Am J Otol* 1999; 20:495–499?
16. Takamiya Y, Friedlander RM, Brem H, Malick A, Martuza RL. Inhibition of angiogenesis and growth of nerve-sheath tumours by AGM-1470. *J Neurosurg* 1993; 78:470–476 28. Fox NC, Freeborough PA. Brain atrophy progression measured from registered serial MRI: validation and application to Alzheimer's disease. *J Magn Reson Imaging*, 1997; 7:1069–1075.
17. Cho Y-D, Choi G-H, Lee S-P, Kim J-K. 1H-MRS metabolic patterns for distinguishing between meningiomas and other brain tumors. *Magn Reson Imaging* 2003; 21:663–672.
18. Tate AR, Majo's C, Moreno A, Howe FA, Griffiths JR, Aru's C. Automated classification of short echo time in vivo 1H brain tumor spectra: a multicenter study. *Magn Reson Med* 2003; 49:29–36.
19. Majo's C, Julia`-Sape' M, Alonso J, Serrallonga M, Aguilera C, Acebes JJ, Aru's C, Gili J. Brain tumor classification by proton MR spectroscopy: comparison of diagnostic accuracy at short and long TE. *Am J Neuroradiol* 2004; 25:1696–1704?
20. E. Haack, et al., *Magnetic Resonance Imaging, Physical Principles and Sequence Design*. Wiley-Liss, New York, 1999.

21. L. Kjaer, P. Ring, C. Thomsen and O. Henriksen. "Texture analysis in quantitative MR imaging", *Acta Radiologica*, Vol 36, No 2, pp. 127-135, 1995.
22. S.C. Bushong, "Magnetic Resonance Images physical and biological principles". Mosby Year Book, New York, NY, 1996.
23. N. B. Karayiannis and Pin-I Pai, "Segmentation of Magnetic Resonance Images Using Fuzzy Algorithms for Learning Vector Quantization", *IEEE Transactions On Medical Imaging*, Vol. 18, No. 2, pp. 172-180, 1999.
24. C. A. Cocosco, A P. Zijdenbos, A. C. Evan, "A Fully Automatic and Robust Brain MRI Tissue Classification Method", *Medical Image Analysis*. Vol.7. No. 4, pp. 513 – 527, 2003.
25. Yongyue Zhang, Michael Brady, and Stephen Smith, Segmentation of Brain MR Images Through a Hidden Markov Random Field Model and the Expectation- Maximization Algorithm, *IEEE Transaction on Medical Imaging*, vol.20, No. 1,2001, pp. 45-57.
26. Rosenberg SI. Natural history of acoustic neuromas. *Laryngoscope* 2000;110:497–508

5/25/2013